Neuroscience 346 (2017) 409–422

CHRONIC DEMYELINATION-INDUCED SEIZURES

ANDREW S. LAPATO, [a,c†] **JENNY I. SZU,** [b†] **JONATHAN P. C. HASSELMANN,** [a] **ANNA J. KHALAJ,** [a] **DEVIN K. BINDER** [a,b,c] **AND SEEMA K. TIWARI-WOODRUFF** [a,b,c*]

[a] *Division of Biomedical Sciences, School of Medicine, University of California Riverside, Riverside, CA 92521, USA*

[b] *Neuroscience Graduate Program, University of California Riverside, Riverside, CA 92521, USA*

[c] *Center for Glial-Neuronal Interactions, University of California Riverside, Riverside, CA 92521, USA*

Abstract—Multiple sclerosis (MS) patients are three to six times more likely to develop epilepsy compared to the rest of the population. Seizures are more common in patients with early onset or progressive forms of the disease and prognosticate rapid progression to disability and death. Gray matter atrophy, hippocampal lesions, interneuron loss, and elevated juxtacortical lesion burden have been identified in MS patients with seizures; however, translational studies aimed at elucidating the pathophysiological processes underlying MS epileptogenesis are limited. Here, we report that cuprizone-mediated chronically demyelinated (9–12 weeks) mice exhibit marked changes to dorsal hippocampal electroencephalography (EEG) and evidence of overt seizure activity. Immunohistochemical (IHC) analyses within the hippocampal CA1 region revealed extensive demyelination, loss of parvalbumin (PV^+) interneurons, widespread gliosis, and changes in aquaporin-4 (AQP4) expression. Our results suggest that chronically demyelinated mice are a valuable model with which we may begin to understand the mechanisms underlying demyelination-induced seizures.

Key words: cuprizone, multiple sclerosis, axon damage, parvalbumin, electroencephalography, hippocampus.

INTRODUCTION

Multiple sclerosis (MS) is an autoimmune demyelinating disorder of the central nervous system (CNS) that affects roughly 2.3 million people worldwide (Browne et al., 2014). In the United States, MS prevalence is estimated at 40–177 people per 100,000 (Evans et al., 2013) and varies with sex, ethnicity, and distance from the equator (Ropper et al., 2014). While MS clinical presentation is multifarious, epidemiological studies show that MS patients are three to six times more likely to develop epileptic seizures than the overall population, with incidence rising with MS duration (Engelsen and Grønning, 1997; Poser and Brinar, 2003; Lund et al., 2014; Marrie et al., 2015). Seizures in MS may signal disease onset or relapse in a subset of patients (Allen et al., 2013; Uribe-San-Martin et al., 2014) and are associated with diminished cognitive function (Calabrese et al., 2012), fulminant disease course, and accelerated time to disability (Martinez-Juarez et al., 2009; Nicholas et al., 2016). However, despite the increased occurrence of seizures among MS patients, little research exists probing their pathogenesis.

Electroencephalography (EEG) recordings from MS patients have revealed aberrant low-amplitude cortical alpha waves and the appearance of delta waves in awake patients (Babiloni et al., 2016), while MS with seizures (MS + S) patients also exhibit waking theta frequencies and paroxysmal discharges (Ghezzi et al., 1990). Magnetic resonance imaging (MRI) of MS + S patients demonstrates abundant temporal leukocortical lesions and hippocampal accumulation of demyelinating foci (Kutzelnigg et al., 2005; Martinez-Lapiscina et al., 2013; Cawley et al., 2015; Calabrese et al., 2016) in addition to findings common in MS, such as global cortical thinning and ventricular hypertrophy (Zivadinov et al., 2016).

Examining postmortem MS + S entorhinal cortex, Nicholas *et al.* reported augmented middle temporal gyrus thinning relative to other cortical regions and layer IV & VI GABAergic interneuron loss not explained by leukocyte infiltration or mitochondrial dysfunction (Nicholas et al., 2016). This is analogous to findings from epileptic hippocampi, which show loss of pyramidal neurons and GABAergic interneurons throughout the hippocampal formation (de Lanerolle et al., 2012; Huusko et al., 2015). Interestingly, MS + S cortical atrophy and neuron loss is localized to structures associated with mesial temporal lobe epilepsy (MTLE) (Calabrese et al., 2012; Nicholas et al., 2016), suggesting convergent pathology between MTLE and MS + S. However, while

*Correspondence to, S.K. Tiwari-Woodruff: Division of Biomedical Sciences, School of Medicine, University of California Riverside, Room 205, 311 School of Medicine Research Building, 900 University Ave, Riverside, CA 92521, USA.
E-mail addresses: seema.tiwari-woodruff@medsch.ucr.edu, seema-tiwari-woodruff@axonremyelination.org (S. K. Tiwari-Woodruff).
† ASL and JIS contributed equally to the preparation of this manuscript and should be considered first co-authors.

Abbreviations: AQP4, aquaporin-4; CC, corpus callosum; CD, cluster of differentiation; CNS, central nervous system; EEG, electroencephalography; GFAP, glial fibrillary acidic protein; IHC, immunohistochemistry; IL, interleukin; MRI, magnetic resonance imaging; MS, multiple sclerosis; MTLE, mesial temporal lobe epilepsy; PV^+, parvalbumin; ROI, region of interest; SO, stratum oriens; vEEG, video-EEG; YFP, yellow fluorescent protein.

http://dx.doi.org/10.1016/j.neuroscience.2017.01.035
0306-4522/

the development of seizures secondary to MS has been probed by a limited number of EEG, MRI, and post-mortem histological studies, little is known regarding its etiology or neuropathology. Furthermore, translational research examining this phenomenon and its origins is restricted to a single study (Hoffmann et al., 2008).

Although several well-established mouse models of MS are available (Merrill, 2009; McCarthy et al., 2012), the cuprizone (bis-cyclohexanone-oxalyldihydrazone; CPZ) diet model was utilized by this study to probe seizures secondary to demyelination. CPZ symptomology is highly reproducible and mirrors clinical features of progressive MS (Lucchinetti et al., 2000; Matsushima and Morell, 2006; Praet et al., 2014). CPZ neuropathology includes axon damage (Kim et al., 2010; Manrique-Hoyos et al., 2012), mitochondrial stress (Praet et al., 2014; Mahad et al., 2015), motor deficits primarily relegated to gait ataxias (Franco-Pons et al., 2007), and easily identifiable tonic–clonic seizures (Hoffmann et al., 2008; Praet et al., 2014). Early reports examining CPZ intoxication noted convulsions in Swiss mice fed $\geqslant$0.3% CPZ for $\geqslant$7 weeks, but did not investigate their pathogenesis (Kesterson and Carlton, 1970, 1983). To our knowledge, only one group has characterized seizures induced by the lower 0.2% concentration of CPZ currently used to model MS (Hoffmann et al., 2008). This group observed unusual spiking in cortical EEG recordings from chronically ($\geqslant$9 weeks) CPZ demyelinated C57BL/6 mice and hippocampal neuron degeneration, but did not identify vulnerable populations or address glial involvement.

To elucidate specific cellular involvement, our group examined CA1 electrophysiology and histopathology in mice subjected to chronic CPZ-induced demyelination. The hippocampal formation frequently exhibits profound changes in MS (Geurts et al., 2007) and MTLE, and has been implicated as a focus of seizure initiation (de Lanerolle et al., 2012) and maintenance (Ellender et al., 2014; Toyoda et al., 2015). These changes include loss of inhibitory interneuron populations, degeneration of CA1 principal neurons, and derangement of dentate gyrus projections into CA regions (de Lanerolle et al., 2012; Liu et al., 2014). For these reasons, we probed CA1 neuronal pathology, including parvalbumin $(PV)^+$ inhibitory interneurons due to this population's vulnerability in demyelination and seizure models (Schwaller et al., 2004; Rossi et al., 2012; Liu et al., 2014).

Glial changes were also assessed, since CPZ induces astrogliosis and phagocyte infiltration at intervals shorter than the chronic model utilized in the present study (Norkute et al., 2009; Skripuletz et al., 2013; Gudi et al., 2014; Praet et al., 2014; Clarner et al., 2015). In addition, both human postmortem tissue and animal models of seizure show reactive astrocytes, which exhibit increased expression of the intermediate filament glial fibrillary acidic protein (GFAP) expression and alterations to channel proteins, including the water channel aquaporin-4 (AQP4) and the inward rectifier potassium channel Kir4.1, both of which are central to epileptogenesis (Oberheim et al., 2008; Anderson and Rodriguez, 2011; Binder et al., 2012; de Lanerolle et al., 2012; Rodriguez-Cruces and Concha, 2015; Nwaobi et al., 2016).

In this study, we characterized EEG waveforms recorded from within the dorsal hippocampus of chronically demyelinated mice with seizures. Our findings indicate that theta and beta frequency power differs with duration of CPZ administration. Additionally, we describe CA1 neuronal and glial histopathology, including infiltration of microglia/macrophages, astrogliosis, changes to AQP4 expression with CPZ duration, pyramidal layer atrophy, and loss of PV^+ interneurons. These results lay a solid foundation for the study of seizure development secondary to demyelination and highlight the necessity for additional research into the pathogenesis of this phenomenon.

EXPERIMENTAL PROCEDURES

Animals

B6.Cg-Tg(Thy1-YFP)16Jrs/J mice backcrossed to wild-type C57BL/6 mice for more than five generations (hereafter referred to as Thy1-YFP mice) were obtained from the Jackson Laboratory (Bar Harbor, ME) and maintained at the University of California Riverside (UCR) animal facility. Originally described by Feng et al. (2000), Thy1-YFP mice express yellow fluorescent protein (YFP) under the control of modified mouse *Thy1* regulatory elements at high levels, resulting in YFP expression in axons, dendrites, and soma of sensory, motor, and some central neurons with no detectable expression in other cell types. Thy1-YFP mice are healthy and have no distinguishable phenotype aside from neuronal YFP expression. All procedures and experiments were conducted in accordance with the National Institutes of Health (NIH) Guide for the Care and Use of Laboratory Animals and approved by the Institutional Animal Care and Use Committee at UCR.

Cuprizone treatment

Eight-week-old male Thy1-YFP mice were assigned to groups that received standard chow (normal; n = 10) or 0.2% cuprizone (CPZ)-milled chow (Harlan Teklad, Madison, WI) as detailed in Crawford et al. (Crawford et al., 2009) for 9 or 12 weeks—hereafter referred to as 9-wk CPZ (n = 10) and 12-wk CPZ (n = 9), respectively. Normal mice received standard chow (Picolab, St. Louis, MO) following the same timeline. All groups had access to food and water *ad libidum* and were housed on a 12-h light/dark cycle under pathogen-free conditions at the UCR animal facility.

EEG probe preparation

A 3-channel twisted bipolar stainless steel electrode was used for all EEG experiments (Plastics One, Roanoke, VA). The bipolar wires were cut to 2 mm in length for intrahippocampal recordings. Similarly, an epidural ground electrode was cut to 0.5 mm and placed during stereotactic surgery (Paxinos and Franklin, 2004). Approximately 0.5 mm of the insulating coat was removed at the distal tip of the bipolar recording electrode using a scalpel to ensure high-fidelity EEG recordings. Implants were sterilized with 70% ethanol and the ground position

on top of the implant pedestal was marked to ensure proper placement of the pins during data acquisition prior to insertion.

EEG implantation

Unilateral indwelling EEG electrodes were chronically implanted in the right dorsal hippocampus after 8 weeks of CPZ or control chow for longitudinal recordings as detailed in (Lee et al., 2012). Mice were anesthetized by intraperitoneal injection of 80 mg/kg ketamine (Phoenix Pharmaceuticals, Burlingame, CA) and 10 mg/kg xylazine (Akorn Inc., Lake Forest, IL). Anesthesia was continuously monitored by testing hind limb paw pinch reflex and additional anesthetics were administered as needed. Body temperature was maintained at 37 °C using a homeothermic pad. Scalp hair was removed using clippers and depilatory cream (Nair; Church Dwight Company, Inc., Trenton, NJ), then disinfected with betadine solution (Purdue Products, Stamford, CT) and cleaned with 70% ethanol.

Mice were immobilized within a stereotaxic frame (Stoelting, Wood Dale, IL) and a midline incision was made and reflected to expose the skull, which was then cleaned with sterile saline and cotton swabs. Etching gel (Kuraray America, New York, NY) was applied to the skull for 10 s, then washed 2–3 times with sterile saline.

EEG electrodes were implanted 1.8 mm caudal and 1.6 mm lateral to bregma to position probe at the right dorsal hippocampus. A 2 mm diameter craniotomy was performed to accommodate the distance between the recording and ground wires using a high-speed surgical hand drill (Foredom, Bethel, CT) equipped with a 1/4-HP-sized carbide bur (SS White, Lakewood, NJ). The skull was cleaned again with sterile saline and the dura was carefully removed using a 27G needle to prevent laceration of the pia or underlying cortex. Bonding agent (Clearfil photo bond; Kuraray America) was prepared according manufacturer instructions and carefully applied on the skull by microbrush to avoid the brain, then cured until completely set. The EEG implant was then secured onto a probe holder with a side clamp and lowered into the hippocampus until the implant pedestal contacted the top of the skull (2 mm per the length of the probe). After verifying that the implant was in place, permanent cement (Panavia SA Cement; Kuraray America) was applied caudal to the implant and skull, then light cured until set. The side clamp was carefully released and the probe holder was raised. Remaining cement was applied in even layers to the exposed skull and the margins of the scalp to ensure a strong hold.

Video-EEG recordings

Treatment groups were separated into two subgroups for staggered video-EEG (vEEG) recordings, which were obtained at weeks 9 and 12 for 4 h per day. Animals 1–3 were recorded on Days 1 and 3, and animals 4–5 were recorded on Days 2 and 4. Control animals were recorded one week after probe implantation. Animals were connected to a tethered EEG recording system via a commutator (Plastics One) connected to a digital EEG acquisition system (MP150, AcqKnowledge 4.4 software) to allow them freedom of motion during data acquisition. Normal EEG output was filtered at 35 Hz (low pass) and 0.1 Hz (high pass) at a gain of 20,000 with a sample rate of 5,000 samples/s. Behavioral activity was recorded using a Sony FDR-AX33 digital video camera (New York, NY) placed in front of the animals' home cages capable of infrared dark phase recording.

EEG analysis

Mice that had no EEG signal due to poor contact of electrodes resulting from chronic recording were excluded from analysis. One mouse was excluded from the normal group (final n = 9) and 3 mice were excluded from the 9 week demyelinated group (final n = 7). No mice were excluded from the 12-wk CPZ group (n = 10). Resting EEG data were analyzed using BrainVision Analyzer 2.1 (Brain Products GmbH, Gilching, Germany). Mice were recorded for 4 h and the entire recording period was analyzed to avoid bias. Artifacts were removed with semi-automatic procedure in BrainVision Analyzer 2.1 software based on gradient, max–min, and low-activity criteria. Resting EEG signals were divided into 1 s segments and Fast Fourier Transform (FFT) was performed on each segment at 1 Hz resolution from 1 to 29 Hz to generate frequency values for each animal in the groups analyzed. Predetermined frequency ranges [Delta (1–4 Hz), Theta (4–7 Hz), Alpha (7–15 Hz), and Beta (15–29 Hz)] were compared by a one-way ANOVA with Tukey's posttest for multiple comparisons.

IHC

After concluding EEG recordings, all mice, regardless of EEG contact strength (Normal n = 10, 9-wk CPZ n = 10, 12-wk CPZ n = 9), were perfusion fixed and processed for IHC (Moore et al., 2014). Briefly, mice were deeply anesthetized by isoflurane inhalation (Piramal Healthcare, Mumbai, India) and perfused transcardially with cold phosphate-buffered saline (PBS, Thermo Fisher Scientific, Waltham, MA) then 10% formalin (Thermo Fisher Scientific). Brains were dissected and post-fixed in 10% formalin (Thermo Fisher Scientific) for 24 h, cryoprotected in 30% sucrose (EMD Millipore, Darmstadt, Germany) for 48 h, and embedded in gelatin for sectioning. 40-μm coronal sections were cut using a HM525 NX cryostat (Thermo Scientific). Sections containing rostral corpus callosum (CC) or dorsal hippocampus were stained by IHC following a previously described protocol (Tiwari-Woodruff et al., 2007; Mangiardi et al., 2011).

Myelination, gliosis, and CA1 pyramidal cell layer neuron densities were visualized by the following primary antibodies at a concentration of 1:500 in PBS unless otherwise noted: chicken anti-myelin basic protein (MBP; polyclonal, EMD Millipore), rabbit anti-olig2 (polyclonal, Thermo Fisher Scientific), mouse anti-cleaved caspase 3 (1:400, clone AM1.31-11, EMD Millipore), mouse anti-glial fibrillary acidic protein (GFAP; clone 1B4, BD Biosciences, San Diego, CA),

rabbit anti-aquaporin 4 (AQP4; polyclonal, EMD Millipore), mouse anti-NeuN (clone A60, EMD Millipore), mouse anti-parvalbumin (PV; 1:400, clone PARV-19, EMD Millipore), mouse anti-adenomatous polyposis coli (CC-1; clone CC-1, Genetex, Irvine, CA), rabbit anti-Ki-67 (1:250, polyclonal, EMD Millipore), and guinea pig anti-doublecortin (DCX; polyclonal, EMD Millipore).

Secondary staining was performed using these polyclonal fluorophore-conjugated antibodies from ThermoFisher Scientific diluted 1:500 unless otherwise noted: goat anti-rabbit IgG (H + L) Cy3 (EMD Millipore), goat anti-mouse IgG (H + L) Alexa Fluor®647 (AF647), goat anti-mouse IgG2a AF647, rabbit anti-goat IgG (H + L) AF647, goat anti-rabbit (H + L) AF647, goat anti-mouse IgG2b AF647, goat anti-guinea pig IgG (EMD Millipore), and donkey anti-chicken IgY Cy3 (EMD Millipore). Nuclei were stained with 4′,6-diamidino-2-phenylindole (DAPI, 2 ng/ml; Molecular Probes) for 15 min after incubation with secondary antibodies and sections were mounted onto positively charged glass slides, allowed to dry, and coverslipped using Fluoromount G mounting medium (Thermo Fisher Scientific).

Confocal microscopy and analysis

CC and hippocampal CA1 contralateral to probe were imaged using an Olympus BX61 confocal microscope (Olympus America Inc., Center Valley, PA) at 10× or 40× magnification. ⩽20 μm thick z-stack projections were compiled using SlideBook 6 software (Intelligent Imaging Innovations, Inc., Denver, CO). Whole coronal section images were acquired at 10× magnification and stitched with Olympus cellSens Software (Olympus America Inc.). Immunostaining was quantified using Fiji version 2.2.0-rc-46/1.50 g (NIH). One data point per stain per animal was entered for each brain region analyzed. To avoid experimenter bias, auto-adjustment of brightness and contrast, as well as threshold of staining signal, was carried out by NIH software. NeuN$^+$, PV$^+$, GFAP$^+$, Olig2$^+$, CC-1$^+$, Thy1-YFP$^+$ blebs, and Ki-67$^+$ cells were quantified by drawing a region of interest (ROI) around a brain structure to be analyzed (CC, CA1 subfields), measuring the area delineated by the ROI, counting immunoreactive cells within the ROI, then counts were normalized to area measured. GFAP, MBP, and DCX immunoreactive signal intensity was determined by Fiji and normalized to area of ROI. Iba1, AQP4, and MBP$^+$ % area was measured as percent positive immunoreactivity within ROIs.

Statistical analysis

Statistical analysis was carried out per previously published work (Tiwari-Woodruff et al., 2007; Crawford et al., 2010). All statistics were performed using Prism 6 software (GraphPad Software, La Jolla, CA). Differences were considered significant at $p \leqslant 0.05$. P values are represented by the following: $^{*}p \leqslant 0.05$, $^{**}p \leqslant 0.01$, $^{***}p \leqslant 0.001$, $^{****}p \leqslant 0.0001$. Effect size ($\eta^2$) is reported as the fraction of the overall variance of all groups pooled attributable to differences among the group means. EEG and IHC data are presented as mean ± SEM and were analyzed by an ordinary one-way ANOVA with Tukey's posttest for multiple comparison test to generate p-values. Number of animals in each group ranged from 7 to 10/group for EEG analysis and 8–12/group for IHC analysis.

RESULTS

Chronic cuprizone demyelination induces behavioral seizures and changes to hippocampal EEG

Thy1-YFP mice fed CPZ for 9 weeks (9-wk CPZ) and 12 weeks (12-wk CPZ) appeared somewhat more active when undisturbed in their home cages relative to standard diet-fed control (normal) mice, but activity level was not quantified. Overall, non-seizure behavioral changes between groups were minimal and have been described previously (Franco-Pons et al., 2007; Praet et al., 2014). Overt seizure-like behavior (Fig. 1A-Seizure) was observed during handling in approximately 30.0% of 8-wk CPZ mice. Seizure behavior increased to 57.5% in 9-wk CPZ mice and 66.25% in 12-wk CPZ mice (n = 20–45 total mice observed over four separate experiments, Fig. 1B). Spontaneous seizures were also recorded in mice unperturbed in their home cages during both light and dark cycles by vEEG (Supplemental Video 1).

Verification and characterization of seizure waveforms in chronically demyelinated mice were performed by intrahippocampal EEG recording. The dorsal hippocampus was selected as the site of electrode implant based on its role in seizure initiation and maintenance (de Lanerolle et al., 2012; Ellender et al., 2014; Toyoda et al., 2015). One week after electrodes were placed, resting state EEG waveforms were acquired to determine if electrical signals corresponded with behavior observed. Mice were awake and freely moving during vEEG recordings (Fig. 1A-EEG Setup).

Significant changes in EEG power were observed with chronic demyelination (Fig. 1 C, D). 9-wk CPZ mice (n = 7) displayed suppressed EEG waveform power compared to normal mice (n = 9), but 12-wk CPZ group (n = 10) waveform power was equivalent to normal (Fig. 1C, D). Theta, alpha, and beta frequencies were significantly increased in 12-wk CPZ mice compared to 9-wk CPZ mice and delta power also trended toward an increase (Fig. 1E; delta p = 0.0573, $\eta^2 = 0.2320$; theta $^{*}p \leqslant 0.05$, $\eta^2 = 0.2928$; alpha $^{*}p \leqslant 0.05$ $\eta^2 = 0.2571$; beta $^{*}p \leqslant 0.05$ $\eta^2 = 0.3203$). EEG data were analyzed by one-way ANOVA with Tukey's posttest for multiple comparisons.

Demyelination occurs in the CC and hippocampus of chronically cuprizone-fed mice

CPZ causes demyelination throughout the CNS by induction of apoptotic pathways in post-mitotic oligodendrocytes (OLs) secondary to mitochondrial dysfunction and accumulation of reactive oxygen species (Mahad et al., 2008; Praet et al., 2014). Montages of coronal brain slices immunostained for myelin basic protein (MBP, green) with nuclei counterstained by 4′,6-diamidino-2-phenylindole (DAPI, red) from normal, 9-wk CPZ and 12-wk CPZ mice showed extensive demyelina-

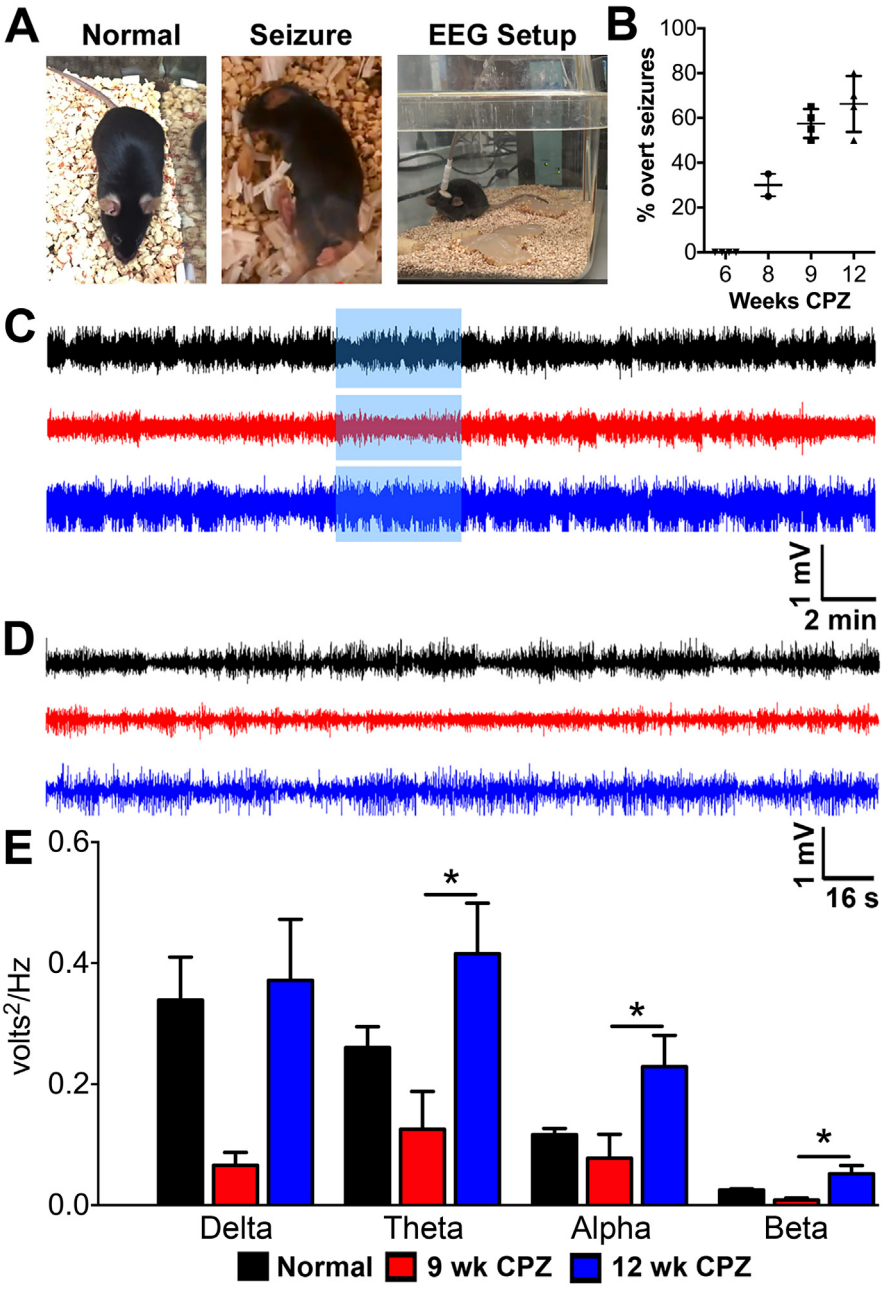

Fig. 1. *Hippocampal electroencephalogram (EEG) changes occur in chronically demyelinated mice*. A) Representative images of a control mouse fed normal diet (normal), an experimental mouse fed cuprizone (CPZ) diet for nine weeks (9-wk CPZ) undergoing seizure-like behavior during handling (seizure), and a normal mouse with an intrahippocampal probe tethered to an external EEG recording setup to allow freedom of movement (EEG setup). B) Nearly 30% of mice on CPZ diet for 8 weeks displayed overt seizure during handling. Seizure activity increased to 55% in 9-wk CPZ mice and 65% in 12-wk CPZ mice (total of 20–45 mice observed over 3 different experiments). C) Representative 30-min recordings from a normal, 9-wk CPZ, & 12-wk CPZ animal. D) Recording period highlighted in blue box from A was magnified to better assess changes in activity. E) Frequency analysis was performed on 4 h of EEG recordings from the same period in normal [n = 9], 9-wk CPZ [n = 7], and 12-wk CPZ [n = 10] groups. No significant changes were observed in any frequency between normal and 9-wk CPZ groups. Similarly, 12-wk CPZ mice showed power equivalent to normal across all frequencies, but exhibited increased theta, alpha, and beta frequency power compared to 9-wk CPZ (theta $^{*}p \leqslant 0.05$, $\eta^2 = 0.2928$; alpha $^{*}p \leqslant 0.05$ $\eta^2 = 0.2571$; beta $^{*}p \leqslant 0.05$ $\eta^2 = 0.3203$, one-way ANOVA with Tukey's posttest for multiple comparisons.

tion in the corpus callosum (CC), cortical hemispheres, and dorsal hippocampus (Hip) (Fig. 2A). A detailed analysis of CC (Fig. 2Bi) and CA1 stratum radiatum (SR) and stratum lacunosum moleculare (SLM) subregions contralateral to EEG implant (Fig. 2Bii) revealed decreased myelin density in the CC (Fig. 2C; 9-wk CPZ vs normal $^{**}p \leqslant 0.01$; 12-wk CPZ vs normal $^{**}p \leqslant 0.01$, $\eta^2 = 0.4373$) and CA1 SR/SLM subregions (Fig. 2G; 9-wk CPZ vs normal $^{****}p < 0.0001$, 12-wk CPZ vs normal $^{****}p < 0.0001$, $\eta^2 = 0.7453$) of CPZ-fed groups.

To investigate the status of OLs in the CNS after chronic demyelination, brain sections were immunostained for the OL lineage-specific transcription factor Olig2 (Meijer et al., 2012). No difference was observed in Olig2$^+$ OL numbers in the CC of any group (Fig. 2Bi, D). Olig2$^+$ OLs were significantly decreased in the CA1 of 12-wk CPZ compared to normal (Fig. 2Bii, H, $^{*}p \leqslant 0.05$, $\eta^2 = 0.2725$).

Post-mitotic OLs were identified by positive immunostaining for both Olig2 and adenomatous polyposis coli (CC-1), a negative regulator of Wnt/β-catenin signaling in myelinating OLs in the CNS (Lang et al., 2013). The number of Olig2$^+$-CC-1$^+$ post-mitotic OLs were decreased by >75% in the CC of 9-wk and 12-wk CPZ groups (Fig. 2E, 9-wk CPZ vs normal $^{****}p < 0.0001$, 12-wk CPZ vs normal $^{****}p < 0.0001$, $\eta^2 = 0.8933$). Similarly, decreased Olig2$^+$CC-1$^+$ OL numbers were observed in the CA1 of 9-wk and 12-wk CPZ mice relative to normal mice (Fig. 2Biv, I, 9-wk CPZ vs normal $^{**}p \leqslant 0.01$, 12-wk CPZ vs normal $^{****}p < 0.0001$, $\eta^2 = 0.5471$).

To assess the status of ongoing apoptosis in OLs due to CPZ, immunostaining for cleaved caspase 3 was performed. In the CC of 9-wk CPZ mice, 46.70 ± 1.784% of Olig2$^+$ OLs exhibited cleaved caspase 3 staining, indicating that these cells were committed to apoptosis (Porter and Janicke, 1999) (Fig. 2F, 9-wk CPZ vs normal $^{****}p < 0.0001$, $\eta^2 = 0.9784$). Similarly, apoptotic cells comprised 46.39 ± 1.661% of total Olig2$^+$ OL lineage cells in the CC of 12-wk CPZ

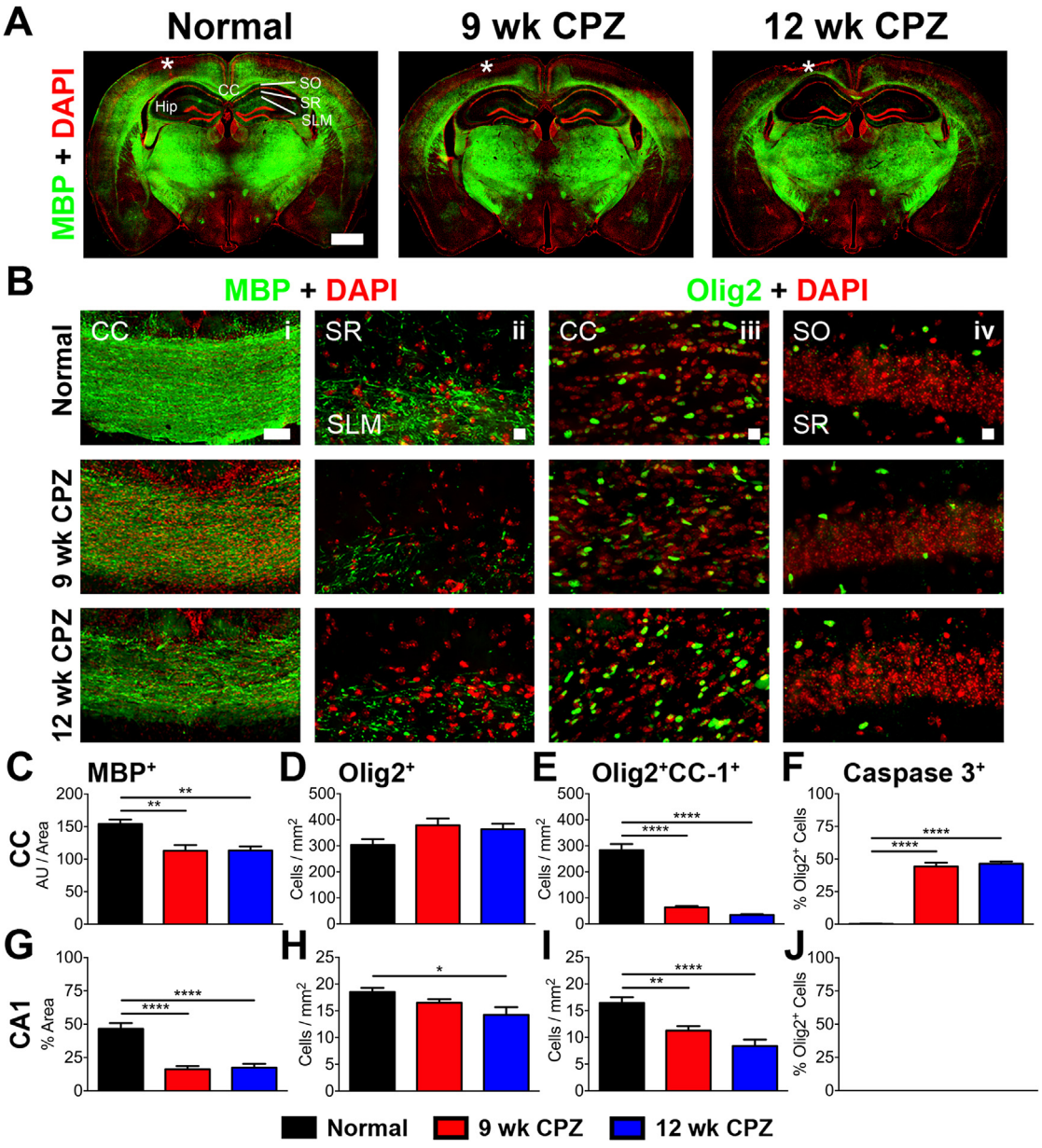

Fig. 2. *Demyelination in the corpus callosum (CC) and hippocampus (Hip) during chronic cuprizone diet.* A) Representative 10X magnification montages of coronal brain sections immunostained for myelin basic protein (MBP, green) and nuclei (DAPI, red) from normal, 9-wk CPZ, and 12-wk CPZ mice show decreased MBP staining in the CC and Hip of 9-wk and 12-wk CPZ mice. Scale bar: 1 mm, * indicates injury at the site of EEG probe implant. B) Representative 10X magnification image of CC, scale bar 100 μm (i) and 40X magnification image of Hip area showing the stratum radiatum (SR) and stratum lacunosum moleculare (SLM) (ii) immunostained for MBP (green) and DAPI (red). A decrease in myelinated fibers was observed in 9-wk and 12-wk CPZ mice. 40X magnification images of the CC (iii) and CA1 (iv) immunostained for Olig2 (green) and DAPI (red) were analyzed for Olig2$^+$ oligodendrocyte (OL) lineage cell numbers. Scale bar in ii, iii, and iv is 10 μm. C) Quantification of MBP staining intensity in the CC normalized to area measured showed a significant decrease in 9-wk CPZ ($^{**}p \leqslant 0.01$) and 12-wk CPZ groups ($^{**}p \leqslant 0.01$) compared to normal mice (n = 8–10 animals/group, one-way ANOVA with Tukey's posttest for multiple comparisons, $\eta^2 = 0.4373$). D) No difference was identified in the number of Olig2$^+$ nuclei counted in the CC of normal, 9-wk CPZ, and 12-wk CPZ mice (n = 7–10 animals/group, one-way ANOVA with Tukey's posttest for multiple comparisons). E) Fewer post-mitotic Olig2$^+$CC-1$^+$ OLs were counted in the CC of 9-wk CPZ ($^{****}p < 0.0001$) and 12-wk CPZ ($^{****}p < 0.0001$) groups as compared to normal mice (n = 7–10 animals/group, one-way ANOVA with Tukey's posttest for multiple comparisons, $\eta^2 = 0.8933$). F) Apoptotic Olig2$^+$ caspase 3$^+$ cells accounted for 44.29 ± 2.879% of all Olig2$^+$ OL lineage cells in the CC of 9-wk CPZ mice (9-wk CPZ vs normal $^{****}p < 0.0001$) and 46.39 ± 1.661% of total Olig2$^+$ OL lineage cells in the CC of 12-wk CPZ mice (12-wk CPZ vs normal $^{****}p < 0.0001$). No difference was observed between 9-wk CPZ and 12-wk CPZ groups (n = 7–10 animals/group, one-way ANOVA with Tukey's posttest for multiple comparisons, $\eta^2 = 0.9784$). G) MBP immunostained areas of CA1 SR/SLM subregions were significantly reduced in 9-wk CPZ ($^{****}p < 0.0001$) and 12-wk CPZ groups ($^{****}p < 0.0001$) compared to normal mice (n = 8–10 animals/group, one-way ANOVA with Tukey's posttest for multiple comparisons, $\eta^2 = 0.7453$). H) No significant change was observed in Olig2 + OLs between normal and 9-wk CPZ mice, but a 20% decrease in Olig2$^+$ OLs was observed in 12-wk CPZ compared to normal mice ($^{*}p \leqslant 0.05$). (n = 8–10 animals/group, one-way ANOVA with Tukey's posttest for multiple comparisons, $\eta^2 = 0.2725$). I) Post-mitotic Olig2$^+$CC-1$^+$ OLs counted in the CA1 were significantly decreased in 9-wk CPZ ($^{**}p \leqslant 0.01$) and 12-wk CPZ mice ($^{****}p < 0.0001$) compared to normal (n = 9–10 animals/group, one-way ANOVA with Tukey's posttest for multiple comparisons, $\eta^2 = 0.5471$). J) Cleaved caspase 3-labeled Olig2$^+$ OL lineage cells were not observed in any groups analyzed (n = 8–10 animals/group, one-way ANOVA with Tukey's posttest for multiple comparisons).

mice (Fig. 2F, 12-wk CPZ vs normal $^{****}p < 0.0001$, $\eta^2 = 0.9784$). Interestingly, although MBP reactivity and Olig2$^+$ OL lineage cells were reduced in the CA1 of 9-wk and 12-wk CPZ mice, cleaved caspase 3 immunoreactivity was not observed in either group (Fig. 2J), indicating that Olig2$^+$ cell loss was caspase 3 independent. IHC data were analyzed by one-way ANOVA with Tukey's posttest for multiple comparisons.

Microglia/macrophage infiltration, astrogliosis, and dysregulation of AQP4 expression

Microglia/macrophages expressing ionized calcium-binding adaptor molecule 1 (Iba1), a cytoplasmic protein constitutively expressed by macrophages and microglia (Ito et al., 1998), occupied 10.44 ± 1.254% of imaged CA1 in normal mice and 13.26 ± 3.270% in 9-wk CPZ mice (Fig. 3C). Iba1$^+$ immunoreactive area increased more than threefold in the CA1 of 12-wk CPZ mice to 47.29 ± 10.98% of imaged fields (Fig. 3C, 12-wk CPZ vs normal $^{**}p \leqslant 0.01$, 12-wk CPZ vs 9-wk CPZ $^{**}p \leqslant 0.01$, $\eta^2 = 0.5128$).

Upregulation of GFAP by reactive astrocytes occurs in the context of inflammatory demyelination and MTLE, confining damage and inflammatory mediators to the area behind the resulting glial scar (Domingues et al., 2016; Robel, 2016). GFAP$^+$ cells in the CA1 of both 9- and 12-wk CPZ groups displayed hypertrophic morphology characteristic of reactive astrocytes, membrane varicosities, and loss of non-overlapping process domains (arrowheads). (Fig. 3B), but these parameters were not quantified. The number of GFAP$^+$ astrocytes significantly increased in the CA1 of 9-wk CPZ ($^{***}p \leqslant 0.001$) and 12-wk CPZ ($^{***}p \leqslant 0.001$) groups compared to normal mice (Fig. 3D, $\eta^2 = 0.5658$). GFAP staining intensity per astrocyte increased in 12-wk CPZ mice compared to normal, indicating increased GFAP expression per cell in the chronically demyelinated CA1 (Fig. 3E, $^{*}p \leqslant 0.05$, $\eta^2 = 0.2514$).

The astrocyte specific water channel AQP4 plays a crucial role in maintaining CNS water and ion homeostasis (Binder et al., 2012; Nagelhus and Ottersen, 2013). Perturbations in AQP4 expression and localization have been identified in postmortem sclerotic hippocampal tissue from epileptic donors (Lee et al., 2004) and translational models of epilepsy (Lee et al., 2012). In normal mice, AQP4 reactivity covered 8.628 ± 0.6162% of the imaged CA1 and followed vasculature (Fig. 3 B). AQP4 immunoreactive area decreased to 4.281 ± 0.4782% in 9-wk CPZ mice, approximately 49% of normal controls ($^{**}p \leqslant 0.01$, $\eta^2 = 0.5668$), but recovered to 10.64 ± 1.297% in 12-wk CPZ mice (Fig. 3F, 12-wk CPZ vs 9-wk CPZ $^{****}p < 0.0001$, $\eta^2 = 0.5668$). IHC data were analyzed by one-way ANOVA with Tukey's posttest for multiple comparisons.

Callosal axon damage, reduced pyramidal cell layer thickness, and loss of PV$^+$ interneurons in the CA1 of chronically demyelinated mice

To assess potential demyelination-induced axon damage, blebbing of axonal plasma membranes, which is associated with toxic protein accumulation (Lesort et al., 1997), was analyzed in chronically demyelinated brain. The coherent linear morphology of Thy1-YFP$^+$ axons observed in the CC of normal mice was lost with chronic demyelination. Thy1-YFP$^+$ axon varicosities, indicative of transected axons or impaired axonal transport, were observed in 9-wk and 12-wk CPZ groups (Fig. 4A, arrowheads). Quantification of axon blebs in the CC (Fig. 4E) showed a significant increase in 9-wk CPZ mice (9-wk CPZ vs normal $^{****}p < 0.0001$, $\eta^2 = 0.9258$) and 12-wk CPZ compared to normal mice (12-wk CPZ vs normal $^{*}p \leqslant 0.05$, $\eta^2 = 0.9258$). Blebbing in 9-wk CPZ mice was significantly higher compared to 12-wk CPZ mice (12-wk CPZ vs 9-wk CPZ $^{****}p < 0.0001$, $\eta^2 = 0.9258$), possibly reflecting loss of Thy1-YFP$^+$ axons in the latter time point. However, no axon or dendrite swelling/blebbing was observed in the SLM or SR of any group (Fig. 4B). CA1 SO projection blebbing was not quantified due to its proximity to the CC, which made distinguishing the two fiber tracts problematic.

Degeneration of hippocampal pyramidal neurons is a feature commonly observed in sclerotic epileptic and MS hippocampi (Ziehn et al., 2010; de Lanerolle et al., 2012). CA1 pyramidal cell layer thickness, measured as height of pyramidal layer nuclei reactive for NeuN, which labels a neuron-specific epitope found on the FOX-3 transcription factor (Mullen et al., 1992), was significantly reduced in the brains of 12-wk CPZ mice relative to normal (Fig. 4C, F; $^{*}p \leqslant 0.05$, $\eta^2 = 0.2458$). However, total NeuN$^+$ pyramidal layer neurons did not change between groups (Fig. 4C, G) and did not co-localize with cleaved caspase 3 in any group examined (not shown), suggesting atrophy of neuronal cell bodies and/or dendrites.

Loss of parvalbumin (PV$^+$) inhibitory interneuron populations occurs in a variety of disease states, including experimental autoimmune encephalomyelitis (an autoimmune mouse model of MS), chemical/traumatic seizure induction, MTLE, and human MS lesions (Arabadzisz et al., 2005; Ziehn et al., 2010; Huusko et al., 2015; Nicholas et al., 2016). PV is expressed by subset of GABAergic interneurons, including basket, axo-axonic, bistratified, and oriens-lacunosum molecular cells in the hippocampus (Schwaller et al., 2004; Liu et al., 2014). Quantification of PV$^+$ inhibitory interneuron soma in the CA1 revealed a significant decrease in 12-wk CPZ mice compared to normal (Fig. 4D, H $^{*}p \leqslant 0.05$, $\eta^2 = 0.4372$). IHC data were analyzed by one-way ANOVA with Tukey's posttest for multiple comparisons.

The effect of chronic demyelination on neuronal regeneration was assessed by immunostaining for doublecortin (DCX), a microtubule associated protein expressed by newly generated neurons (Rao and Shetty, 2004) and Ki-67, a nuclear protein expressed by proliferating cells (Kee et al., 2002). DCX$^+$ cells were not observed in the CA1 pyramidal cell layer of normal mice. However, DCX$^+$ cells with stellate morphology appeared in the CA1 SO and overlying white matter tract of 9-wk CPZ ($^{****}p < 0.0001$) and 12-wk CPZ ($^{**}p \leqslant 0.001$) mice, but did not penetrate the pyramidal

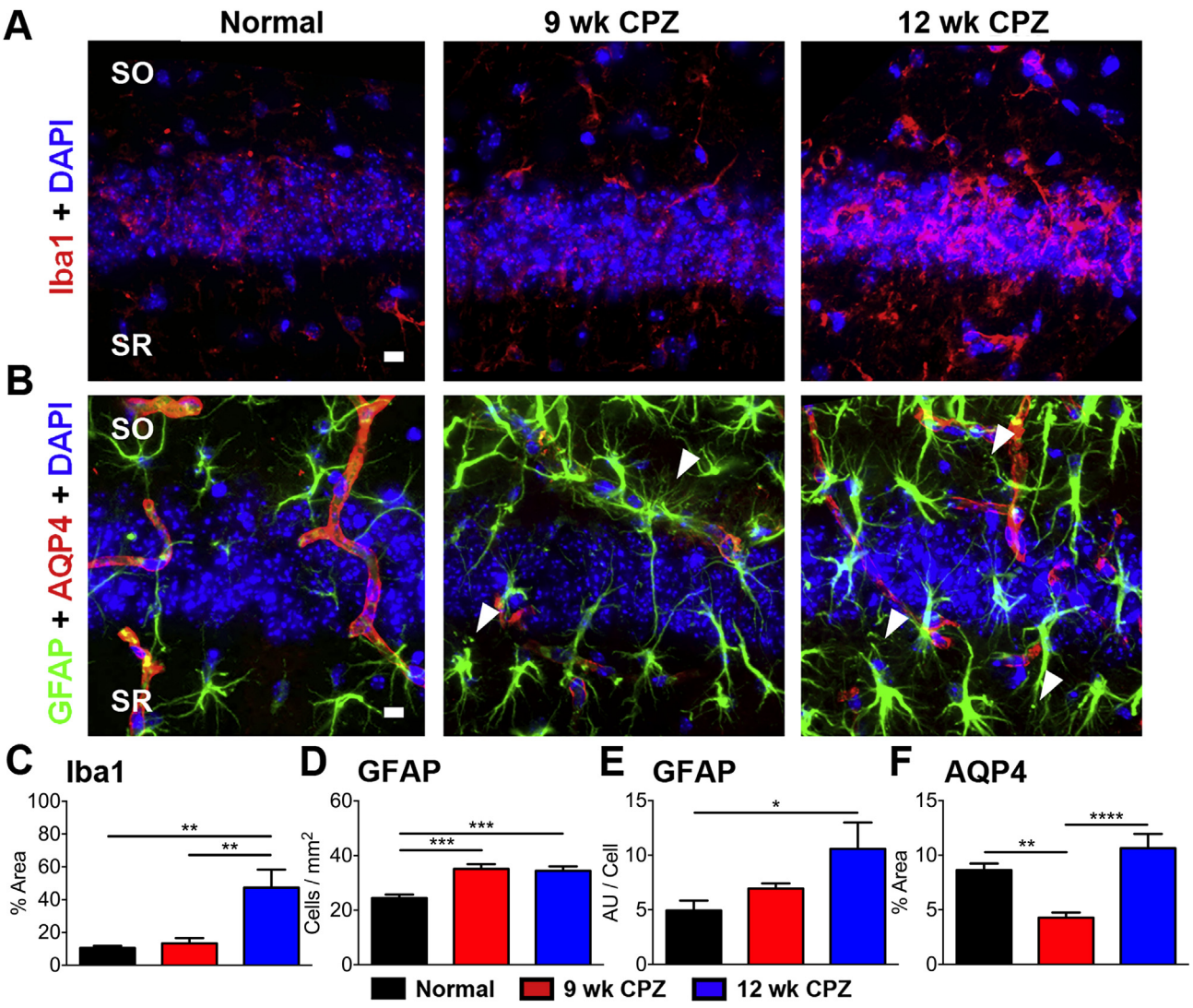

Fig. 3. *Macrophage/microglia infiltration, reactive astrocytes, and altered AQP4 expression are observed in the CA1 of chronically cuprizone-fed mice with seizures.* A) Representative 40X magnification images of Iba1 (red)- and DAPI (blue)-immunostained CA1 stratum oriens (SO)/SR from normal, 9-wk CPZ, and 12-wk CPZ mouse coronal brain sections show increased Iba1 reactivity in 12-wk CPZ mice. Scale bar: 10 μm. B) Representative 40X magnification images of GFAP (green), AQP4 (red) immunostaining, and DAPI (blue) stained CA1 SO/SR of normal, 9-wk CPZ, and 12-wk CPZ mice. The number of GFAP$^+$ astrocytes and staining intensity per cell increased in the CA1 of 9-wk and 12-wk CPZ mice and displayed hypertrophic morphology characteristic of reactive astrocytes, membrane varicosities, and loss of non-overlapping process domains (arrowheads). In normal mice, AQP4$^+$ staining followed vasculature and co-localized with GFAP at the site of astrocyte end foot processes contacting blood vessels. AQP4 staining decreased in 9-wk CPZ mice, but GFAP staining increased proximal to vasculature. AQP4 reactive area returned to normal levels in 12-wk CPZ mice and GFAP$^+$ reactive astrocytes did not accumulate near blood vessels. Scale bar: 10 μm. C) Iba1$^+$ immunostaining in the CA1 was quantified as a percent of imaged field in normal, 9-wk CPZ, and 12-wk CPZ mice. Iba1$^+$ microglia/macrophages occupied approximately 10–13% of the imaged CA1 in normal and 9-wk CPZ mice, but increased more than threefold in 12-wk CPZ mice to 47.29 ± 10.98% (12-wk CPZ vs normal, $^{**}p \leqslant 0.01$; 12-wk CPZ vs 9-wk CPZ $^{**}p \leqslant 0.01$; n = 7–9 animals/group, one-way ANOVA with Tukey's posttest for multiple comparisons, $\eta^2 = 0.5128$). D,E) Astrocytes were quantified by counting the number of GFAP$^+$ cells/area. A significant increase was observed in the CA1 of 9-wk CPZ ($^{***}p \leqslant 0.001$) and 12-wk CPZ (($^{***}p \leqslant 0.001$) groups compared to normal mice. GFAP staining intensity (represented in arbitrary units "AU") per astrocyte also rose significantly in 12-wk CPZ mice compared to normal mice $^{*}p \leqslant 0.05$), indicating increased GFAP expression per cell (n = 8–10 animals/group, one-way ANOVA with Tukey's posttest for multiple comparisons; GFAP$^+$ cells/mm^2 $\eta^2 = 0.5658$; GFAP intensity per cell $\eta^2 = 0.2514$). F) AQP4 immunoreactive area was significantly decreased in the CA1 of 9-wk CPZ mice compared to normal ($^{**}p \leqslant 0.01$) and 12-wk CPZ groups ($^{****}p < 0.0001$; n = 7–10 animals/group, one-way ANOVA with Tukey's posttest for multiple comparisons, $\eta^2 = 0.5668$).

cell layer (Fig. 5A, B, $\eta^2 = 0.6077$). Ki-67$^+$ nuclei were rarely observed in all groups analyzed and did not co-localize with DCX$^+$ cells. These data indicate that new neurons did not account for unchanged pyramidal cell numbers despite pyramidal layer thinning and reduced PV$^+$ staining during chronic demyelination.

DISCUSSION

Despite increased seizure incidence in MS patients (Evans et al., 2013), little is known regarding the pathophysiology or risk factors that contribute to epileptogenesis in these patients. We have for the first time

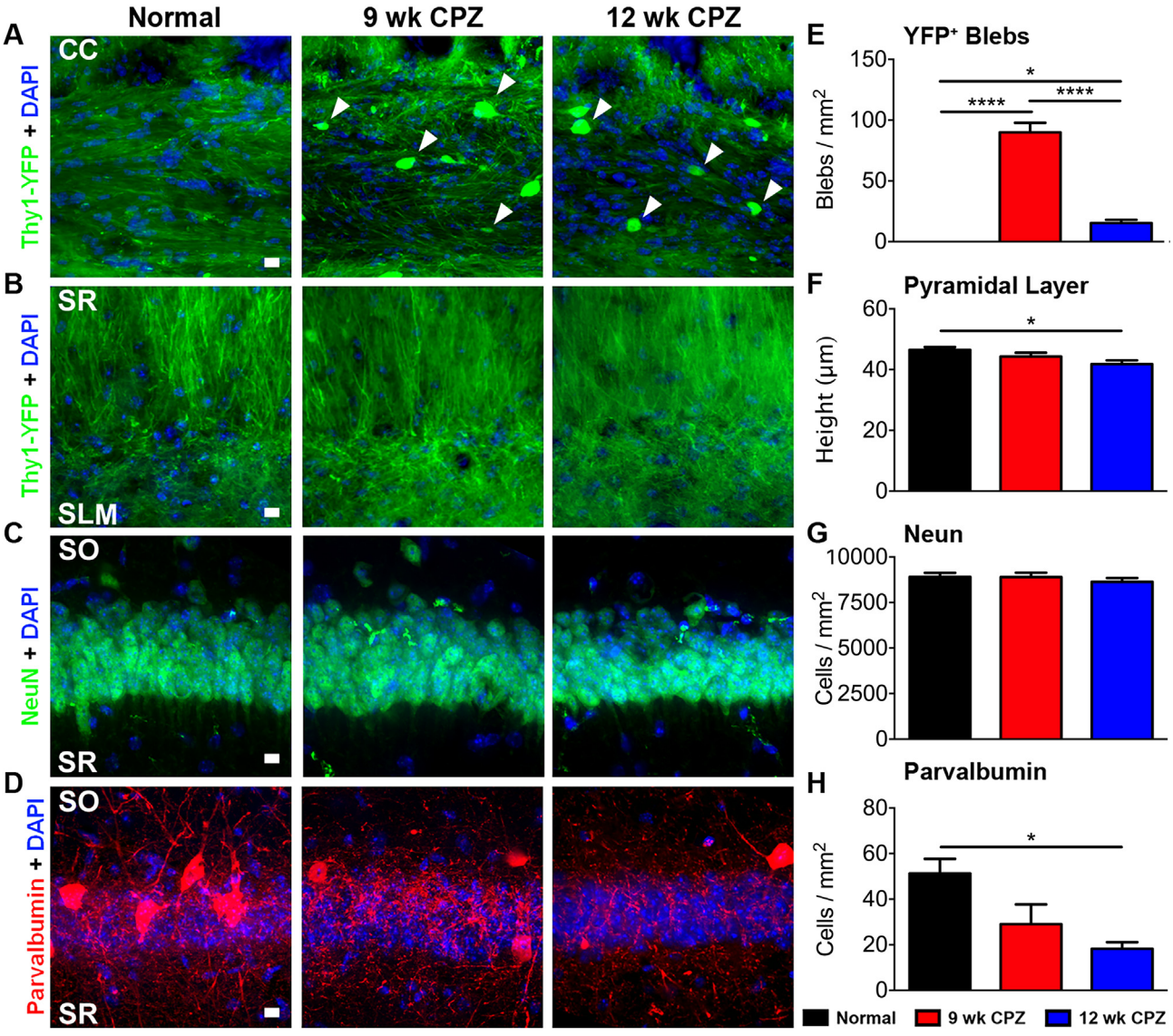

Fig. 4. *CC axon pathology, reduced CA1 pyramidal cell layer thickness, and loss of PV immunostaining in the CA1 of chronically demyelinated mice with seizures.* A,B) Representative 40X magnification images from normal, 9-wk CPZ, and 12-wk CPZ coronal brain sections showing the CC and the SR/SLM regions of the CA1. The coherent linear morphology of Thy1-YFP$^+$ axons in the normal CC was lost with chronic demyelination. Thy1-YFP$^+$ axon varicosities (arrowheads), indicative of transected axons or impaired protein transport, were observed in 9-wk and 12-wk CPZ groups. No axon or dendrite swelling/blebbing was observed in SR or SLM. Scale bar: 10 μm. C,D) Representative 40X magnification images of CA1 pyramidal layer immunostained for NeuN+ (green), DAPI, (blue), and parvalbumin (PV; red) from normal, 9-wk CPZ and 12-wk CPZ groups. A decrease in overall CA1 pyramidal neuron layer thickness and loss of PV$^+$ neurons was observed in 9-wk CPZ and 12-wk CPZ CA1 pyramidal layer. Scale bars: 10 μm. E) Quantification of axon blebs in the CC showed a significant increase in both 9- and 12-wk CPZ groups compared to the normal group (9-wk CPZ vs normal $^{****}p < 0.0001$; 12-wk CPZ vs normal $^{*}p \leqslant 0.05$). Blebbing in the CC of 9-wk CPZ mice was significantly higher than 12-wk CPZ mice ($^{****}p < 0.0001$), reflecting fewer Thy1-YFP callosal axons (n = 8–10 animals/group, one-way ANOVA with Tukey's posttest for multiple comparisons, $\eta^2 = 0.9258$). F,G) Quantification of pyramidal cell layer thickness was determined by measuring the total height of NeuN$^+$ nuclei in the pyramidal cell layer. Compared to normal mice, a significant decrease was observed in pyramidal cell layer thickness of 12-wk CPZ mice ($^{*}p \leqslant 0.05$). However, total pyramidal layer NeuN+ neurons were not statistically different between groups (n = 8–10 animals/group, one-way ANOVA with Tukey's posttest for multiple comparisons; pyramidal layer height $\eta^2 = 0.2458$). H) Quantification of PV$^+$ interneuron soma in the CA1 region pyramidal cell layer showed a significant decrease in 12-wk CPZ mice $^{*}p \leqslant 0.05$) as compared to normal group (n = 8–10 animals/group, one-way ANOVA with Tukey's posttest for multiple comparisons, $\eta^2 = 0.4372$).

demonstrated that long-term CPZ administration reproduces facets of neuropathology observed in human MS patients with seizures (Martinez-Lapiscina et al., 2013; Nicholas et al., 2016). We observed changes in intrahippocampal EEG recordings from chronically demyelinated mice that experienced spontaneous seizures during chronic CPZ treatment. Specifically, we found a reduction in EEG power at the 9-week time point, which may reflect the electrophysiological effects of widespread cortical demyelination. Interestingly, we observed recovery of EEG power at the 12-week time point. Future studies will need to assess the timing of onset of spontaneous elec-

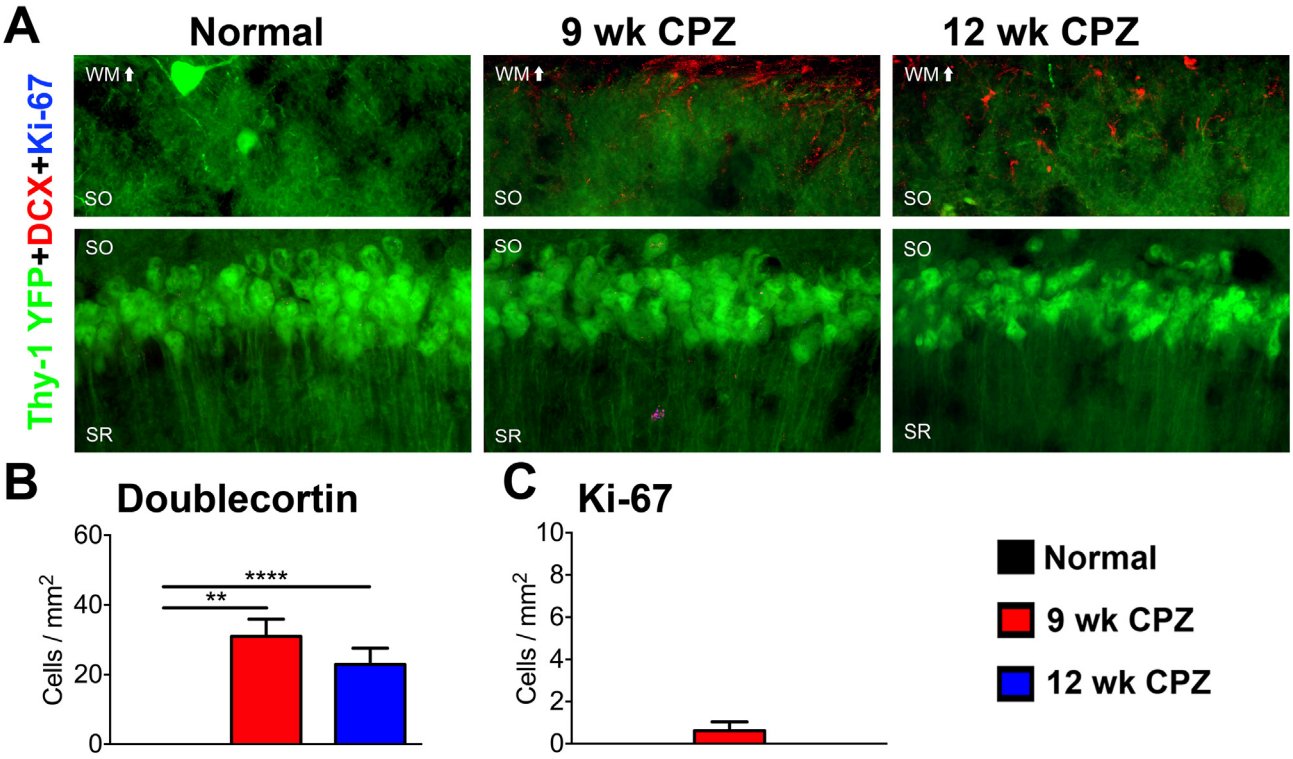

Fig. 5. *Status of Ki-67$^+$ and doublecortin$^+$ cell populations in the CA1 of chronically demyelinated mice with seizures.* A) Representative 40X magnification images of the CA1 pyramidal cell layer immunostained for doublecortin (DCX) and Ki-67 in normal, 9-wk CPZ, and 12-wk CPZ mice. DCX$^+$ cells with stellate morphology were observed in the CA1 SO and overlying white matter tract of 9-wk CPZ and 12-wk CPZ mice. Ki-67$^+$ nuclei were rarely detected in the CA1 of any group and did not co-localize with DCX. Scale bar: 10 μm. B) DCX$^+$ cell numbers were significantly increased in the CA1 SO of 9-wk CPZ ($^{****}p < 0.0001$) and 12-wk CPZ mice mice ($^{**}p \leqslant 0.01$; n = 8–9 animals/group, one-way ANOVA with Tukey's post test for multiple comparisons, $\eta^2 = 0.6077$). C) Ki-67$^+$ nuclei numbers were not significantly different between groups (n = 8–9 animals/group, one-way ANOVA with Tukey's posttest for multiple comparisons).

trographic seizures in this model as well as the relationship of seizure onset to demyelination and other cellular and molecular changes.

While the pathophysiology leading to seizures in chronic demyelination remains to be elucidated, our results indicate several possibilities. Loss of CA1 PV$^+$ interneuron cell bodies suggests impaired inhibition may contribute to seizures during demyelination. PV$^+$ inhibitory interneurons comprise an essential component of the hippocampal timing circuitry crucial to maintaining physiologic seizure resistance (Schwaller et al., 2004; Huusko et al., 2015; Wolf et al., 2016). Our results mirror models of seizure disorders (Hernandez-Lain et al., 2013; Houser, 2014; Liu et al., 2014; Huusko et al., 2015) and autoimmune inflammatory demyelination (Ziehn et al., 2010), where drop-out of PV$^+$ immunoreactivity is also observed. Future studies will examine whether CA1 inhibitory interneuron loss is confined to PV$^+$ cells or extends to other GABAergic populations, such as cholecystokinin octapeptide$^+$ cells which are thought to represent a distinct inhibitory network (Kohus et al., 2016).

CPZ intoxication does not contribute to neuronal pathology directly (Praet et al., 2014). Neuron sparing in the face of mitochondrial stress imposed by CPZ has been explained by metabolic coupling to astrocytes, which augment neuronal resilience by carrying out glycolysis in response to energetic deficits (Dewar et al., 2003; Marrif and Juurlink, 2003; Praet et al., 2014). In addition to increased numbers of GFAP$^+$ reactive astrocytes, astrocytes displayed crossed domains, membrane blebbing, upregulation of GFAP, and altered AQP4 expression with chronic demyelination concurrent with changes to theta and beta frequency power and spontaneous seizure. Membrane blebbing of astrocyte processes has been shown to precede apoptotic cell death following oxygen-glucose deprivation (Gouix et al., 2014), and is associated with impaired ATP metabolism in other cell types (Lemasters et al., 1987). However, whether blebbing observed reflects impaired metabolism or pre-apoptotic astrocytes requires additional investigation.

Recent research illustrates the importance of astrocyte-astrocyte and astrocyte-oligodendrocyte gap junction coupling in maintaining astrocyte homeostatic function and survival (Magnotti et al., 2011). Genetic ablation of connexin-30 and connexin-43, two gap junction proteins responsible for oligodendrocyte-astrocyte coupling, leads to marked astrogliosis, myelin vacuolation, and tonic–clonic seizures (Magnotti et al., 2011). While astrogliosis begins early with CPZ administration (Gudi et al., 2014), in the chronically demyelinated CNS, loss of astrocyte-oligodendrocyte coupling via gap junctions could feasibly contribute to the seizures and pathological astrocyte morphology that our group observed. In addition, increased expression of the astrocyte gap junction

protein connexin-43 and more rapid decay of inward glutamate currents in astrocytes have been shown to accompany kainic acid-induced seizures (Takahashi et al., 2010). These changes occur prior to alteration of astrocyte inward potassium currents, indicating that changes in astrocyte coupling with other glia and glutamate buffering may herald the onset of spontaneous seizures in that model. Future studies will probe the extent to which changes in astrocyte-oligodendrocyte gap junctions are featured in the genesis of seizures in chronic CPZ-mediated demyelination and what consequences these changes may have on glutamate and potassium handling.

Mounting evidence suggests that downregulation of AQP4 is observed in seizure models and may play a role in hyperexcitability leading to seizures (Binder et al., 2012; Alvestad et al., 2013; Hubbard et al., 2016). Specifically, AQP4 appears to be downregulated during the epileptogenic period in which spontaneous seizures emerge (Lee et al., 2012; Alvestad et al., 2013; Hubbard et al., 2016). Our results showed a similar pattern, with a transient decrease in CA1 AQP4 expression at 9 weeks of demyelination at the earliest onset of observable seizures, then rising at 12 weeks once seizures were well established. Changes in aquaporin expression may be significant as their expression has been shown to trace Kir4.1 localization in astrocytes, implicating the co-involvement of these two molecules in regulating osmolarity that could contribute to perturbation of resting membrane potential and hyperexcitability (Binder et al., 2012) by increasing extracellular potassium concentration. Additional study is necessary to identify whether alterations to Kir4.1/AQP4 homeostasis contribute to seizure genesis in chronic demyelination. In addition, chronic video-EEG monitoring will be needed to determine the exact time course of spontaneous seizure onset in the CPZ model and the focus of seizure initiation (hippocampus *vs.* cortex) (Hoffmann et al., 2008).

The appearance of augmented $Iba1^+$ immunoreactivity coinciding with seizures and changes to EEG theta and beta frequency power is congruous with findings from both translational models of epilepsy and analysis of postmortem human tissue (Zhang et al., 2016; Eyo et al., 2017). Infiltration of microglia/-macrophages peaks at 4.5 weeks of CPZ intoxication as is mediated by the chemokines CCL2, CCL3, and CXCL10 (Clarner et al., 2015). However, to the best of our knowledge, no studies have addressed microglia/macrophage behavior in the chronic CPZ model utilized in this study. In mouse models of epilepsy, microglia/macrophages express so-called M1 pro-inflammatory cytokines such as inducible nitric oxide synthase, tumor necrosis factor α, interleukin (IL)-1β, IL-6, and IL-12 as well as lymphocyte co-stimulatory molecules cluster of differentiation (CD) 80, CD86, and major histocompatibility complex II at high levels (Eyo et al., 2017). M1 polarization may be attributable to signaling by TLR4/MYD88 and purinergic receptors, which play a prominent role in many neuroinflammatory states (Zhou et al., 2013; Hu and Mao, 2016). Determining the phenotype of microglia/macrophages that appear in CA1 during chronic demyelination may help clarify their role in seizures secondary to MS.

Additional research is required to elucidate the pathophysiology underpinning inhibitory cell loss in chronic demyelination with seizures. However, based on our data, it is conceivable that chronic demyelination-induced metabolic dysfunction arising in astrocytes due to oxidative stress or uncoupling from post-mitotic oligodendrocytes could preclude their ability to execute neuroprotective functions such as maintaining physiologic osmolarity and metabolite buffering, thereby leading to loss of vulnerable PV^+ neuron and seizures. The resulting release of ATP and inflammatory mediators from hippocampal neurons susceptible to excitotoxic death may then attract microglia/macrophages. Future studies will address the functional correlations of our results, while brain tissue from MS + S patients will be evaluated for markers observed in the present study to establish translational relevance.

Understanding the pathophysiology contributing to seizures in chronic demyelinating disease has implications extending beyond the treatment of MS with epilepsy. Oligodendrocyte death and dysmyelination are frequently noted features of seizure disorders. If a relationship exists between these phenomena and hippocampal GABAergic neuron survival, exposing this framework could inform investigation into novel therapeutic targets in epilepsy and MS that could prevent seizure-induced demyelination and/or demyelination-induced seizures.

AUTHOR CONTRIBUTIONS

ASL and JIS contributed equally to the preparation of this manuscript and should be considered first co-authors.

ASL, JIS, AJK, and JPCH performed the experiments;

ASL, JIS, SKTW, and DKB analyzed the data;

ASL, JIS, DKB, AJK, JPCH, and SKTW wrote the manuscript.

COMPETING FINANCIAL INTERESTS

The authors declare that they have no competing financial interests.

Acknowledgments—This work was generously supported by the National Multiple Sclerosis Society Grants NMSS-RG-4853A3/2 and NIH R01-7R01NS081141 Grants to S.K.T.-W.

REFERENCES

Allen AN, Seminog OO, Goldacre MJ (2013) Association between multiple sclerosis and epilepsy: large population-based record-linkage studies. BMC Neurol 13:189.

Alvestad S, Hammer J, Hoddevik EH, Skare O, Sonnewald U, Amiry-Moghaddam M, Ottersen OP (2013) Mislocalization of AQP4 precedes chronic seizures in the kainate model of temporal lobe epilepsy. Epilepsy Res 105:30–41.

Anderson G, Rodriguez M (2011) Multiple sclerosis, seizures, and antiepileptics: role of IL-18, IDO, and melatonin. Eur J Neurol 18:680–685.

Arabadzisz D, Antal K, Parpan F, Emri Z, Fritschy JM (2005) Epileptogenesis and chronic seizures in a mouse model of temporal lobe epilepsy are associated with distinct EEG

patterns and selective neurochemical alterations in the contralateral hippocampus. Exp Neurol 194:76–90.
Babiloni C, Del Percio C, Capotosto P, Noce G, Infarinato F, Muratori C, Marcotulli C, Bellagamba G, Righi E, Soricelli A, Onorati P, Lupattelli T (2016) Cortical sources of resting state electroencephalographic rhythms differ in relapsing-remitting and secondary progressive multiple sclerosis. Clin Neurophysiol 127:581–590.
Binder DK, Nagelhus EA, Ottersen OP (2012) Aquaporin-4 and epilepsy. Glia 60:1203–1214.
Browne P, Chandraratna D, Angood C, Tremlett H, Baker C, Taylor BV, Thompson AJ (2014) Atlas of Multiple Sclerosis 2013: A growing global problem with widespread inequity. Neurology 83:1022–1024.
Calabrese M, Grossi P, Favaretto A, Romualdi C, Atzori M, Rinaldi F, Perini P, Saladini M, Gallo P (2012) Cortical pathology in multiple sclerosis patients with epilepsy: a 3 year longitudinal study. J Neurol Neurosur Ps 83:49–54.
Calabrese M, Castellaro M, Bertoldo A, De Luca A, Pizzini FB, Ricciardi GK, Pitteri M, Zimatore S, Magliozzi R, Benedetti MD, Manganotti P, Montemezzi S, Reynolds R, Gajofatto A, Monaco S (2016) Epilepsy in multiple sclerosis: the role of temporal lobe damage. Mult Scler.
Cawley N, Solanky BS, Muhlert N, Tur C, Edden RA, Wheeler-Kingshott CA, Miller DH, Thompson AJ, Ciccarelli O (2015) Reduced gamma-aminobutyric acid concentration is associated with physical disability in progressive multiple sclerosis. Brain 138:2584–2595.
Clarner T, Janssen K, Nellessen L, Stangel M, Skripuletz T, Krauspe B, Hess FM, Denecke B, Beutner C, Linnartz-Gerlach B, Neumann H, Vallieres L, Amor S, Ohl K, Tenbrock K, Beyer C, Kipp M (2015) CXCL10 triggers early microglial activation in the cuprizone model. J Immunol 194:3400–3413.
Crawford DK, Mangiardi M, Tiwari-Woodruff SK (2009) Assaying the functional effects of demyelination and remyelination: revisiting field potential recordings. J Neurosci Meth 182:25–33.
Crawford DK, Mangiardi M, Song B, Patel R, Du S, Sofroniew MV, Voskuhl RR, Tiwari-Woodruff SK (2010) Oestrogen receptor beta ligand: a novel treatment to enhance endogenous functional remyelination. Brain: J Neurol 133:2999–3016.
de Lanerolle NC, Lee TS, Spencer DD (2012) Histopathology of human epilepsy. In: Noebels JL, Avoli M, Rogawski MA, Olsen RW, Delgado-Escueta AV, editors. Jasper's basic mechanisms of the epilepsies. Bethesda (MD): National Center for Biotechnology Information (US).
Dewar D, Underhill SM, Goldberg MP (2003) Oligodendrocytes and ischemic brain injury. J Cereb Blood Flow Metab 23:263–274.
Domingues HS, Portugal CC, Socodato R, Relvas JB (2016) Oligodendrocyte, astrocyte, and microglia crosstalk in myelin development, damage, and repair. Front Cell Dev Biol 4:71.
Ellender TJ, Raimondo JV, Irkle A, Lamsa KP, Akerman CJ (2014) Excitatory effects of parvalbumin-expressing interneurons maintain hippocampal epileptiform activity via synchronous afterdischarges. J Neurosci 34:15208–15222.
Engelsen BA, Grønning M (1997) Epileptic seizures in patients with multiple sclerosis. Is the prognosis of epilepsy underestimated? Seizure 6:377–382.
Evans C, Beland SG, Kulaga S, Wolfson C, Kingwell E, Marriott J, Koch M, Makhani N, Morrow S, Fisk J, Dykeman J, Jette N, Pringsheim T, Marrie RA (2013) Incidence and prevalence of multiple sclerosis in the Americas: a systematic review. Neuroepidemiology 40:195–210.
Eyo UB, Murugan M, Wu LJ (2017) Microglia-neuron communication in epilepsy. Glia 65:5–18.
Feng G, Mellor RH, Bernstein M, Keller-Peck C, Nguyen QT, Wallace M, Nerbonne JM, Lichtman JW, Sanes JR (2000) Imaging neuronal subsets in transgenic mice expressing multiple spectral variants of GFP. Neuron 28:41–51.
Franco-Pons N, Torrente M, Colomina MT, Vilella E (2007) Behavioral deficits in the cuprizone-induced murine model of demyelination/remyelination. Toxicol Lett 169:205–213.
Geurts JJ, Bo L, Roosendaal SD, Hazes T, Daniels R, Barkhof F, Witter MP, Huitinga I, van der Valk P (2007) Extensive hippocampal demyelination in multiple sclerosis. J Neuropathol Exp Neurol 66:819–827.
Ghezzi A, Montanini R, Basso PF, Zaffaroni M, Massimo E, Cazzullo CL (1990) Epilepsy in multiple sclerosis. Eur Neurol 30:218–223.
Gouix E, Buisson A, Nieoullon A, Kerkerian-Le Goff L, Tauskela JS, Blondeau N, Had-Aissouni L (2014) Oxygen glucose deprivation-induced astrocyte dysfunction provokes neuronal death through oxidative stress. Pharmacol Res 87:8–17.
Gudi V, Gingele S, Skripuletz T, Stangel M (2014) Glial response during cuprizone-induced de- and remyelination in the CNS: lessons learned. Front Cell Neurosci 8:73.
Hernandez-Lain A, Hedley-Whyte ET, Hariri LP, Molyneaux B, Nagle KJ, Cole AJ, Kilbride R (2013) Pathology of bilateral pulvinar degeneration following long duration status epilepticus. Seizure 22:901–904.
Hoffmann K, Lindner M, Groticke I, Stangel M, Loscher W (2008) Epileptic seizures and hippocampal damage after cuprizone-induced demyelination in C57BL/6 mice. Exp Neurol 210:308–321.
Houser CR (2014) Do structural changes in GABA neurons give rise to the epileptic state? Adv Exp Med Biol 813:151–160.
Hu QP, Mao DA (2016) Histone deacetylase inhibitor SAHA attenuates post-seizure hippocampal microglia TLR4/MYD88 signaling and inhibits TLR4 gene expression via histone acetylation. BMC Neurosci 17:22.
Hubbard JA, Szu JI, Yonan JM, Binder DK (2016) Regulation of astrocyte glutamate transporter-1 (GLT1) and aquaporin-4 (AQP4) expression in a model of epilepsy. Exp Neurol 283:85–96.
Huusko N, Romer C, Ndode-Ekane XE, Lukasiuk K, Pitkanen A (2015) Loss of hippocampal interneurons and epileptogenesis: a comparison of two animal models of acquired epilepsy. Brain Struct Funct 220:153–191.
Ito D, Imai Y, Ohsawa K, Nakajima K, Fukuuchi Y, Kohsaka S (1998) Microglia-specific localisation of a novel calcium binding protein, Iba1. Brain Res Mol Brain Res 57:1–9.
Kee N, Sivalingam S, Boonstra R, Wojtowicz JM (2002) The utility of Ki-67 and BrdU as proliferative markers of adult neurogenesis. J Neurosci Meth 115:97–105.
Kesterson JW, Carlton WW (1970) Aqueductal stenosis as the cause of hydrocephalus in mice fed the substituted hydrazine, cuprizone. Exp Mol Pathol 13:281–294.
Kesterson JW, Carlton WW (1983) Cuprizone toxicosis in mice—attempts to antidote the toxicity. Toxicol Appl Pharm 22:6–13.
Kim JY, Shen S, Dietz K, He Y, Howell O, Reynolds R, Casaccia P (2010) HDAC1 nuclear export induced by pathological conditions is essential for the onset of axonal damage. Nat Neurosci 13:180–189.
Kohus Z, Kali S, Rovira-Esteban L, Schlingloff D, Papp O, Freund TF, Hajos N, Gulyas AI (2016) Properties and dynamics of inhibitory synaptic communication within the CA3 microcircuits of pyramidal cells and interneurons expressing parvalbumin or cholecystokinin. J Physiol 594:3745–3774.
Kutzelnigg A, Lucchinetti CF, Stadelmann C, Bruck W, Rauschka H, Bergmann M, Schmidbauer M, Parisi JE, Lassmann H (2005) Cortical demyelination and diffuse white matter injury in multiple sclerosis. Brain 128:2705–2712.
Lang J, Maeda Y, Bannerman P, Xu J, Horiuchi M, Pleasure D, Guo F (2013) Adenomatous polyposis coli regulates oligodendroglial development. J Neurosci 33:3113–3130.
Lee TS, Eid T, Mane S, Kim JH, Spencer DD, Ottersen OP, de Lanerolle NC (2004) Aquaporin-4 is increased in the sclerotic hippocampus in human temporal lobe epilepsy. Acta Neuropathol 108:493–502.
Lee DJ, Hsu MS, Seldin MM, Arellano JL, Binder DK (2012) Decreased expression of the glial water channel aquaporin-4 in the intrahippocampal kainic acid model of epileptogenesis. Exp Neurol 235:246–255.
Lemasters JJ, DiGuiseppi J, Nieminen AL, Herman B (1987) Blebbing, free Ca2+ and mitochondrial membrane potential preceding cell death in hepatocytes. Nature 325:78–81.

Lesort M, Terro F, Esclaire F, Hugon J (1997) Neuronal APP accumulates in toxic membrane blebbings. J Neural Transm 104:497–513.
Liu YQ, Yu F, Liu WH, He XH, Peng BW (2014) Dysfunction of hippocampal interneurons in epilepsy. Neurosci Bull 30:985–998.
Lucchinetti C, Bruck W, Parisi J, Scheithauer B, Rodriguez M, Lassmann H (2000) Heterogeneity of multiple sclerosis lesions: implications for the pathogenesis of demyelination. Ann Neurol 47:707–717.
Lund C, Nakken KO, Edland A, Celius EG (2014) Multiple sclerosis and seizures: incidence and prevalence over 40 years. Acta Neurol Scand 130:368–373.
Magnotti LM, Goodenough DA, Paul DL (2011) Deletion of oligodendrocyte Cx32 and astrocyte Cx43 causes white matter vacuolation, astrocyte loss and early mortality. Glia 59:1064–1074.
Mahad D, Ziabreva I, Lassmann H, Turnbull D (2008) Mitochondrial defects in acute multiple sclerosis lesions. Brain 131:1722–1735.
Mahad DH, Trapp BD, Lassmann H (2015) Pathological mechanisms in progressive multiple sclerosis. Lancet Neurol 14:183–193.
Mangiardi M, Crawford DK, Xia X, Du S, Simon-Freeman R, Voskuhl RR, Tiwari-Woodruff SK (2011) An animal model of cortical and callosal pathology in multiple sclerosis. Brain Pathol 21:263–278.
Manrique-Hoyos N, Jurgens T, Gronborg M, Kreutzfeldt M, Schedensack M, Kuhlmann T, Schrick C, Bruck W, Urlaub H, Simons M, Merkler D (2012) Late motor decline after accomplished remyelination: impact for progressive multiple sclerosis. Ann Neurol 71:227–244.
Marrie RA, Reider N, Cohen J, Trojano M, Sorensen PS, Cutter G, Reingold S, Stuve O (2015) A systematic review of the incidence and prevalence of sleep disorders and seizure disorders in multiple sclerosis. Mult Scler:342–349.
Marrif H, Juurlink BHJ (2003) Differential vulnerability of oligodendrocytes and astrocytes to hypoxic-ischemic stresses. Adv Mol Cell Biol:857–867. Elsevier.
Martinez-Juarez IE, Lopez-Meza E, Gonzalez-Aragon Mdel C, Ramirez-Bermudez J, Corona T (2009) Epilepsy and multiple sclerosis: increased risk among progressive forms. Epilepsy Res 84:250–253.
Martinez-Lapiscina EH, Ayuso T, Lacruz F, Gurtubay IG, Soriano G, Otano M, Bujanda M, Bacaicoa MC (2013) Cortico-juxtacortical involvement increases risk of epileptic seizures in multiple sclerosis. Acta Neurol Scand 128:24–31.
Matsushima GK, Morell P (2006) The neurotoxicant, cuprizone, as a model to study demyelination and remyelination in the central nervous system. Brain Pathol 11:107–116.
McCarthy DP, Richards MH, Miller SD (2012) Mouse models of multiple sclerosis: experimental autoimmune encephalomyelitis and Theiler's virus-induced demyelinating disease. Methods Mol Biol 900:381–401.
Meijer DH, Kane MF, Mehta S, Liu H, Harrington E, Taylor CM, Stiles CD, Rowitch DH (2012) Separated at birth? The functional and molecular divergence of OLIG1 and OLIG2. Nat Rev Neurosci 13:819–831.
Merrill JE (2009) In vitro and in vivo pharmacological models to assess demyelination and remyelination. Neuropsychopharmacology 34:55–73.
Moore SM, Khalaj AJ, Kumar S, Winchester Z, Yoon J, Yoo T, Martinez-Torres L, Yasui N, Katzenellenbogen JA, Tiwari-Woodruff SK (2014) Multiple functional therapeutic effects of the estrogen receptor β agonist indazole-Cl in a mouse model of multiple sclerosis. Proc Natl Acad Sci U S A 111:18061–18066.
Mullen RJ, Buck CR, Smith AM (1992) NeuN, a neuronal specific nuclear protein in vertebrates. Development 116:201–211.
Nagelhus EA, Ottersen OP (2013) Physiological roles of aquaporin-4 in brain. Physiol Rev 93:1543–1562.
Nicholas R, Magliozzi R, Campbell G, Mahad D, Reynolds R (2016) Temporal lobe cortical pathology and inhibitory GABA interneuron cell loss are associated with seizures in multiple sclerosis. Mult Scler 22:25–35.
Norkute A, Hieble A, Braun A, Johann S, Clarner T, Baumgartner W, Beyer C, Kipp M (2009) Cuprizone treatment induces demyelination and astrocytosis in the mouse hippocampus. J Neurosci Res 87:1343–1355.
Nwaobi SE, Cuddapah VA, Patterson KC, Randolph AC, Olsen ML (2016) The role of glial-specific Kir4.1 in normal and pathological states of the CNS. Acta Neuropathol 132:1–21.
Oberheim NA, Tian GF, Han X, Peng W, Takano T, Ransom B, Nedergaard M (2008) Loss of astrocytic domain organization in the epileptic brain. J Neurosci 28:3264–3276.
Paxinos G, Franklin KBJ (2004) The mouse brain in stereotaxic coordinates. Elsevier Academic Press.
Porter AG, Janicke RU (1999) Emerging roles of caspase-3 in apoptosis. Cell Death Differ 6:99–104.
Poser CM, Brinar VV (2003) Epilepsy and multiple sclerosis. Epilepsy Behav 4:6–12.
Praet J, Guglielmetti C, Berneman Z, Van der Linden A, Ponsaerts P (2014) Cellular and molecular neuropathology of the cuprizone mouse model: clinical relevance for multiple sclerosis. Neurosci Biobehav Rev 47:485–505.
Rao MS, Shetty AK (2004) Efficacy of doublecortin as a marker to analyse the absolute number and dendritic growth of newly generated neurons in the adult dentate gyrus. Eur J Neurosci 19:234–246.
Robel S (2016) Astroglial scarring and seizures: a cell biological perspective on epilepsy. Neuroscientist.
Rodriguez-Cruces R, Concha L (2015) White matter in temporal lobe epilepsy: clinico-pathological correlates of water diffusion abnormalities. Quant Imaging Med Surg 5:264–278.
Ropper AH, Samuels MA, Klein JP (2014) Chapter 36. Multiple sclerosis and other inflammatory demyelinating diseases. In: Adams and victor's principles of neurology, 10e. New York, NY: The McGraw-Hill Companies.
Rossi S, Studer V, Motta C, De Chiara V, Barbieri F, Bernardi G, Centonze D (2012) Inflammation inhibits GABA transmission in multiple sclerosis. Mult Scler 18:1633–1635.
Schwaller B, Tetko IV, Tandon P, Silveira DC, Vreugdenhil M, Henzi T, Potier MC, Celio MR, Villa AE (2004) Parvalbumin deficiency affects network properties resulting in increased susceptibility to epileptic seizures. Mol Cell Neurosci 25:650–663.
Skripuletz T, Hackstette D, Bauer K, Gudi V, Pul R, Voss E, Berger K, Kipp M, Baumgartner W, Stangel M (2013) Astrocytes regulate myelin clearance through recruitment of microglia during cuprizone-induced demyelination. Brain 136:147–167.
Takahashi DK, Vargas JR, Wilcox KS (2010) Increased coupling and altered glutamate transport currents in astrocytes following kainic-acid-induced status epilepticus. Neurobiol Dis 40:573–585.
Tiwari-Woodruff S, Morales LB, Lee R, Voskuhl RR (2007) Differential neuroprotective and antiinflammatory effects of estrogen receptor (ER)alpha and ERbeta ligand treatment. Proc Natl Acad Sci U S A 104:14813–14818.
Toyoda I, Fujita S, Thamattoor AK, Buckmaster PS (2015) Unit activity of hippocampal interneurons before spontaneous seizures in an animal model of temporal lobe epilepsy. J Neurosci 35:6600–6618.
Uribe-San-Martin R, Ciampi-Diaz E, Suarez-Hernandez F, Vasquez-Torres M, Godoy-Fernandez J, Carcamo-Rodriguez C (2014) Prevalence of epilepsy in a cohort of patients with multiple sclerosis. Seizure 23:81–83.
Wolf DC, Bueno-Junior LS, Lopes-Aguiar C, Do Val Da.Silva RA, Kandratavicius L, Leite JP (2016) The frequency of spontaneous seizures in rats correlates with alterations in sensorimotor gating, spatial working memory, and parvalbumin expression throughout limbic regions. Neuroscience 312:86–98.
Zhang B, Zou J, Han L, Rensing N, Wong M (2016) Microglial activation during epileptogenesis in a mouse model of tuberous sclerosis complex. Epilepsia 57:1317–1325.
Zhou M, Wang CM, Yang WL, Wang P (2013) Microglial CD14 activated by iNOS contributes to neuroinflammation in cerebral ischemia. Brain Res 1506:105–114.

Ziehn MO, Avedisian AA, Tiwari-Woodruff S, Voskuhl RR (2010) Hippocampal CA1 atrophy and synaptic loss during experimental autoimmune encephalomyelitis, EAE. Lab Invest 90:774–786.

Zivadinov R, Uher T, Hagemeier J, Vaneckova M, Ramasamy DP, Tyblova M, Bergsland N, Seidl Z, Dwyer MG, Krasensky J, Havrdova E, Horakova D (2016) A serial 10-year follow-up study of brain atrophy and disability progression in RRMS patients. Mult Scler 22:1709–1718.

APPENDIX A. SUPPLEMENTARY DATA

Supplementary data associated with this article can be found, in the online version, at http://dx.doi.org/10.1016/j.neuroscience.2017.01.035.

(Received 31 October 2016, Accepted 23 January 2017)
(Available online 30 January 2017)